Int. J. Heat Mass Transfer. Vol. 26, No. 7, pp. 1037–1053, 1983
Printed in Great Britain

0017-9310/83 $3.00 + 0.00

ANALYSIS AND COMPUTATION OF THREE-DIMENSIONAL, TRANSIENT FLOW AND COMBUSTION THROUGH GRANULATED PROPELLANTS

N. C. MARKATOS and D. KIRKCALDY
Concentration Heat and Momentum Ltd, Bakery House, 40 High Street, Wimbledon, London SW19 5AU, U.K.

(*Received* 6 *April* 1982 *and in final form* 4 *November* 1982)

Abstract—Gas-permeable solid propellants possess great potential for producing high thrusts during extremely short time intervals. This paper presents the theoretical formulation and application of a model describing the important physical phenomena taking place in both gaseous and solid phases in such three-dimensional, two-phase, unsteady, reactive flow systems, as found in internal ballistics. A stable, fast-converging, fully-implicit numerical method, was used to solve the coupled, non-linear differential equations of the model, so that effects of importance to the internal-ballistics designer can be studied. Solutions are presented that predict the pressure-wave build-up and accelerating flame-front for beds of granulated solid propellants in gun barrels with an accelerating projectile. The results show that the flame-front accelerates and the rate of pressurisation increases substantially in the downstream direction, as expected, and are physically reasonable in every respect.

NOMENCLATURE

a_i, finite-domain coefficients;
a_1, a_2, heat transfer parameters for the gaseous and solid phase, respectively (heat transfer coefficients times the interphase area) [W K^{-1}];
A_s, total surface area of particles in a control cell [m^2];
b, co-volume of gas [m^3 kg^{-1}];
$\dot{b}$, burning rate of particles [kg m^{-2} s^{-1}];
C_f, interphase friction coefficient;
C_1, C_2, specific heats of gas and particles, respectively [J kg^{-1} K^{-1}];
D, particle diameter [m];
f, interphase friction factor;
g, acceleration of gravity [m s^{-2}];
$\tilde{h}_1, \tilde{h}_2$, stagnation enthalpies of gas and particles, respectively [J kg^{-1}];
h_c, chemical energy of propellant [J kg^{-1}];
K, intergranular stress proportionality constant [N m^{-2}];
$\dot{m}_{21}$, rate of interphase mass transfer [kg s^{-1}];
$\dot{m}'''_{21}$, rate of interphase mass transfer per unit volume [kg m^{-3} s^{-1}];
n, propellant burning rate index;
p, P, gas and particle pressures, respectively [N m^{-2}];
$\dot{q}_{12}, \dot{q}_{1s}, \dot{q}_{s2}$, rates of heat transfer from gas to particles, from gas to the particle surface, and from the particle surface to the particle interior, respectively [W];
r, radial coordinate;
R, radial extent of gun barrel [m];
$\bar{R}$, specific gas constant [J kg^{-1} K^{-1}];
R_1, R_2, gas and particle volume fractions;
R_2^*, 'shadow' particle volume fraction;
s, a linear particle dimension [m];
S_ϕ, source term for variable ϕ;
t, time [s];
T_1, T_2, gas and particle temperatures, respectively [K];
T_∞, initial temperature at particle centre [K];
T_s, particle surface temperature [K];
T_{ign}, propellant ignition temperature [K];
$u_1, u_2, v_1, v_2, w_1, w_2$, velocities of gas and particles in the azimuthal, radial and axial directions [m s^{-1}];
V, volume of control cell [m^3];
y, a space coordinate;
z, axial coordinate.

Greek symbols

γ, specific heat ratio of gas;
Γ_ϕ, diffusion coefficient for variable ϕ;
δ, the thermal wave penetration depth in a spherical particle [m];
ε, propellant burning-rate proportionality constant [kg m^{-2} s^{-1}];
θ, angular coordinate;
ρ_1, ρ_2, gas and particle densities, respectively [kg m^{-3}];
τ, intergranular stress [N m^{-2}];
ϕ, a general dependent variable.

Subscripts

0, initial condition;
1, refers to the gas-phase;
2, refers to the solid-phase;
s, refers to the interphase.

1. INTRODUCTION

1.1. *The problem considered and its practical relevance*

THE PRESENT study is concerned with the prediction of the transient phenomena following ignition of granular propellants. The following transient phenomena occur

in a few milliseconds: penetration of hot gases into the voids between the granules, convective heating of granules to ignition, granule compaction and rapid pressurisation. The mass generated in the ignition region accelerates the flame forward, with the region behind the flame rapidly increasing in pressure as more and more mass is being generated. The problem of flame spreading and of possible shock-front formation in porous propellant charges is obviously important in the design and analysis of propulsion systems, and in predicting transition to detonation of granular explosives. Further applications of the present study may be found also in any engineering application that involves fluidised-bed combustion.

1.2. *Objectives of the study*

The ability to calculate 3-dim., transient dynamics resulting from pressure wave formation and flame spreading in a bed of small grain propellant is the motivation for this work. Therefore, the objectives of the study are: (a) to formulate a theoretical model describing the important physical phenomena involved in both gaseous and solid phases during combustion of solid propellants, which allows solutions under all conditions of practical relevance; (b) to solve the associated equations by a stable, fast convergent numerical algorithm (first proposed in ref. [1], and first applied in ref. [2]); and, (c) to demonstrate the physical realism of results obtained for typical problems.

1.3. *Previous work and present contribution*

The physical and chemical processes taking place in internal ballistics phenomena are complex, and their experimental study is difficult to perform and subject to high degrees of uncertainty and inaccuracy. Due to the above complexities, several theoretical approaches, most restricted to 1-dim. situations, have been proposed.

The theoretical methods can be classified into four categories: (1) statistical models [3–5]; (2) continuum-mechanics models [6, 7]; (3) formal averaging models [8]; and (4) two-phase fluid dynamics model [9]. The advantages and disadvantages of each of the above methods have been analysed [10–12] and a comprehensive review basis has been provided [18].

The method employed in this study is the continuum-mixture approach of refs. [13, 14, 19], which is developed by formulating the governing equations on the basis that mass, momentum and energy fluxes are balanced over control volumes occupied by *space-sharing interspersed continua.* According to this concept, distinct phases (e.g. gas and particles) are present within the same space (although never at precisely the same time), their shares of space being measured by their 'volume fractions'.

2. THEORETICAL MODEL

2.1. *The physical problem*

The basic features of the gun barrel are outlined in Fig. 1. A cylindrical domain is considered, enclosed by the gun barrel and the base of the projectile, and containing a solid propellant in powder form and a gas. The solid propellant comes in various shapes and sizes. In the past, propellants in cord form were in favour. The present-day propellants are still cord-shaped but with slotted tubes. However, spherical forms cannot be ruled out [11] and this is the form assumed in this study.†

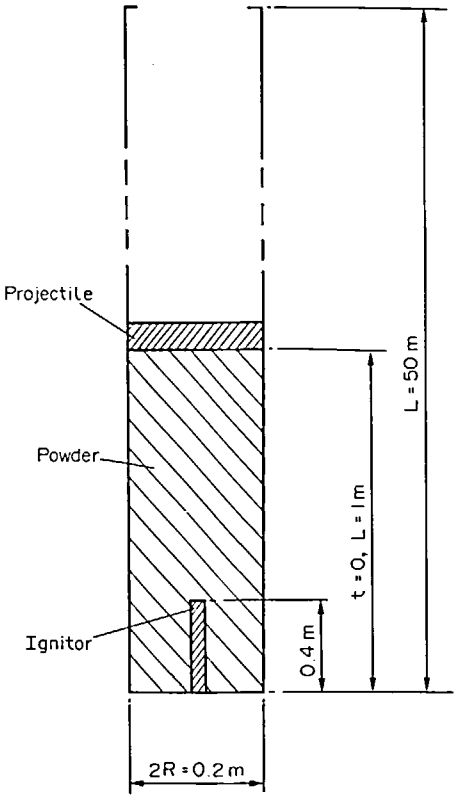

FIG. 1. The gun barrel considered.

Ignition is provided by inflow of hot gas at the base of the cylinder. The gas is forced into the granular bed through a multiply-perforated nozzle; this causes a compaction of the granular bed near the entrance region, and also heats up the nearby granular propellants to ignition. The so-ignited propellants give off more hot gases which are pushed forward by the pressure gradient to ignite more propellants. Thus, a steep pressure gradient is created inside the combustion chamber and the accelerated gaseous products cause the shell to move.

The quantitative formulation of such unsteady, two-phase flow phenomena requires, apart from the unsteady multi-phase gas-dynamic equations, the utilisation of associated empirical correlations for

† This assumption is made for analytical simplicity of the interphase heat- and mass-transfer correlations used in the present application [e.g. see equation (15)]. However, the method is applicable to propellants of other shapes as well, provided that the surface to volume ratio of the solid is given or can be calculated.

interphase friction factors, interphase heat transfer factors, and burning-rate laws for the rate of interphase mass transfer.

2.2. *The dependent and independent variables*

The following are the dependent variables of the problem: velocities of gas and particles in the radial, azimuthal and axial directions: v_1, v_2, u_1, u_2, w_1 and w_2; pressure, p; gas and particle volumetric concentrations, R_1, R_2; and, enthalpies of gas and particles, $\tilde{h}_1$ and $\tilde{h}_2$.

The independent variables are: the radial, circumferential and axial distances, r, θ, z, in a polar-cylindrical coordinate system; and, the time, t.

2.3. *The partial differential equations*

In order to study the transient phenomena in the granular propellant bed, the following set of governing equations describing the change of mass, momentum and energy for the gas phase and the change of mass, momentum and energy for the solid phase are derived:

2.3.1. *The mass-conservation equations.* The volume fractions, densities and velocities of each of the two phases must, in order to satisfy the mass-conservation principle, obey the following equations:

gas-phase mass equation

$$\frac{\partial}{\partial t}(\rho_1 R_1)+\frac{\partial}{\partial z}(\rho_1 R_1 w_1)+\frac{1}{r}\frac{\partial}{\partial r}(\rho_1 R_1 r v_1) + \frac{1}{r}\frac{\partial}{\partial \theta}(\rho_1 R_1 u_1) = \dot{m}'''_{21}, \quad (1)$$

particle-phase mass equation

$$\frac{\partial}{\partial t}(\rho_2 R_2)+\frac{\partial}{\partial z}(\rho_2 R_2 w_2)+\frac{1}{r}\frac{\partial}{\partial r}(\rho_2 R_2 r v_2) + \frac{1}{r}\frac{\partial}{\partial \theta}(\rho_2 R_2 u_2) = -\dot{m}'''_{21} \quad (2)$$

where $\dot{m}'''_{21}$ is the rate of mass transfer per unit volume from the solid phase to the gaseous phase, due to gasification of solid particles. The volumetric fractions are related by the 'space-sharing' equation,

$$R_1 + R_2 = 1. \quad (3)$$

2.3.2. *The conservation of momentum equations.*

$$\frac{\partial}{\partial t}(\rho_i R_i \phi)+\frac{1}{r}\frac{\partial}{\partial r}(r R_i \rho_i v_i \phi)+\frac{1}{r}\frac{\partial}{\partial \theta}(R_i \rho_i u_i \phi) + \frac{\partial}{\partial z}(R_i \rho_i w_i \phi) = \frac{1}{r}\frac{\partial}{\partial r}\left(r R_i \Gamma_\phi \frac{\partial \phi}{\partial r}\right) + \frac{1}{r}\frac{\partial}{\partial \theta}\left(R_i \Gamma_\phi \frac{\partial \phi}{\partial \theta}\right)+\frac{\partial}{\partial z}\left(R_i \Gamma_\phi \frac{\partial \phi}{\partial z}\right)+S_\phi \quad (4)$$

where ϕ stands for u_1, u_2, v_1, v_2, w_1 and w_2; Γ_ϕ and S_ϕ are diffusion coefficients and source terms; and subscript i refers to the phase in question (gaseous or solid). For the application of the model considered in this paper diffusion effects are considered negligible ($\Gamma_\phi = 0$). The source terms S_ϕ are given in Table 1, in the form in which they occur in the finite-difference equations, e.g. as the integral over the finite-difference cells.

The formulation of the pressure terms has occasioned some uncertainty among writers on the subject, and it is sometimes thought that different pressures ought to be provided for each phase. It is not especially useful to do so. Therefore, a single pressure appears in *both* equations, and an additional 'intergranular-force' term in *one* of the equations. This term arises from the 'particle-packing' equation, governing the pressure in the solid phase as its volume fraction approaches the physically attainable limit,

$$P = p + \tau(R_2), \quad (5)$$

wherein the solid phase sustains the extra stress τ, this being a function of the volume fraction, R_2.

Further inspection of the above equations reveals that the term $p(\partial R_1/\partial y)$, which frequently occurs in the literature, is missing. This is because use of $\partial/\partial y\,(R_1 p)$ instead of $R_1(\partial p/\partial y)$ is simply erroneous. A term like $p(\partial R_1/\partial y)$ implies the presence of a momentum source *proportional to pressure* whenever R_1 is non-uniform. There is no physical mechanism which can produce it. A change in the general *pressure level* would alter such a source.

2.3.3. *The conservation of energy equations.* Let $\tilde{h}_1, \tilde{h}_2$ stand for the stagnation enthalpy of the gas and solid phases per unit mass, respectively, by which is meant the thermodynamic enthalpy plus the kinetic energy of the phase plus any potential energy associated with the position of the fluid in a force field. Then, the first law of

Table 1. Source terms in momentum equations

ϕ	$\int S_\phi \mathrm{dvol}$ (Integral source term for finite-difference cell)
w_1	$VR_1(\rho_1 g - \partial p/\partial z) + C_f(w_2 - w_1) + \dot{m}_{21} w_2$
w_2	$VR_2(\rho_2 g - \partial p/\partial z) + C_f(w_1 - w_2) - \dot{m}_{21} w_2 - \dfrac{\partial R_2 \tau}{\partial z}$
	V is cell volume; C_f is interphase friction coefficient and τ is intergranular stress (see Section 2.4).
v_1	$VR_1\left(\dfrac{\rho_1 u_1^2}{r} - \dfrac{\partial p}{\partial r}\right) + C_f(v_2 - v_1) + \dot{m}_{21} v_2$
v_2	$VR_2\left(\dfrac{\rho_2 u_2^2}{r} - \dfrac{\partial p}{\partial r}\right) + C_f(v_1 - v_2) - \dot{m}_{21} v_2 - \dfrac{\partial R_2 \tau}{\partial r}$
$u_1 r$	$-VR_1 \dfrac{\partial p}{\partial \theta} + C_f r(u_2 - u_1) + \dot{m}_{21} u_2 r$
$u_2 r$	$-VR_2 \dfrac{\partial p}{\partial \theta} + C_f r(u_1 - u_2) - \dot{m}_{21} u_2 r - \dfrac{\partial R_2 \tau}{\partial \theta}$
	The equation for the angular momentum, ur, is solved in preference to that for u

thermodynamics leads to the following equations:

gas-phase energy equation

$$\frac{\partial}{\partial t}[(\rho_1\tilde{h}_1-p)R_1]+\frac{1}{r}\frac{\partial}{\partial r}(rR_1\rho_1v_1\tilde{h}_1)$$
$$+\frac{1}{r}\frac{\partial}{\partial\theta}(R_1\rho_1u_1\tilde{h}_1)+\frac{\partial}{\partial z}(\rho_1R_1w_1\tilde{h}_1)$$
$$=C_f(v_2-v_1)v_2+C_f(w_2-w_1)w_2+C_f(u_2-u_1)u_2$$
$$-\dot{q}_{12}+\dot{m}'''_{21}\left(h_s+\frac{v_1^2}{2}+\frac{w_1^2}{2}+\frac{u_1^2}{2}\right)-p\frac{\partial R_1}{\partial t}, \quad (6)$$

particle-phase energy equation

$$\frac{\partial}{\partial t}[(\rho_2\tilde{h}_2-P)R_2]+\frac{1}{r}\frac{\partial}{\partial r}(rR_2\rho_2v_2\tilde{h}_2)$$
$$+\frac{1}{r}\frac{\partial}{\partial\theta}(R_2\rho_2u_2\tilde{h}_2)+\frac{\partial}{\partial z}(\rho_2R_2w_2\tilde{h}_2)$$
$$=C_f(v_1-v_2)v_1+C_f(w_1-w_2)w_1+C_f(u_1-u_2)u_1$$
$$+\dot{q}_{12}-\dot{m}'''_{21}\left(h_s+\frac{v_2^2}{2}+\frac{w_2^2}{2}+\frac{u_2^2}{2}\right)-P\frac{\partial R_2}{\partial t} \quad (7)$$

where $\dot{q}_{12}$ is rate of heat transfer from gas to particles; $h_s=\tilde{h}_2+h_c$ where h_c is the heat of combustion of the solid particles, and $P=p+\tau$.

2.3.4. *The particle-size calculation.* For the problems under consideration it is necessary to calculate the distribution throughout the field of the average local size of the particles. This necessity arises because, for example, the rate of burning may depend strongly upon the size of the particles; and this size diminishes, of course, as the particles are consumed.

The approach followed is to compute a 'shadow' volume fraction, R_2^*, that is to say, the volume fraction which the solid phase would have possessed, at each point, in the absence of combustion; the velocities, however, being the same as the phase actually possesses. Therefore, R_2^* obeys an equation, which is identical to equation (2), but for the absence of the mass-transfer rate, $\dot{m}'''_{21}$ ($\dot{m}'''_{21}=0$).

The particle size can now be deduced from

$$\frac{s}{s_0}=\left(\frac{R_2}{R_2^*}\right)^{1/3} \quad (8)$$

where s stands for some linear dimension of the particle, and s_0 is the value of s for the particles initially. Knowledge of s then permits the local values of interphase heat-transfer coefficient, interphase friction coefficient, and mass-transfer rate to be determined.

Equations (1), (2), (4), (6), (7) and that for R_2^* form a system of twelve coupled, non-linear, partial differential equations.

2.4. *Auxiliary relations*

The above set of differential equations has to be solved in conjunction with observance of constraints on the values of the variables, represented by algebraic relations.

The constitutive relations used for the reported application of the model follow. Except for interphase heat transfer, these relations follow the lines of refs. [7, 8, 18]. However, because the purpose of this paper is to describe the theoretical method and the nature of the results, rather than to quantify them in detail, some of these relations have been considerably simplified. It should be mentioned that, although little emphasis is placed on these relations at present, their proper form and function are essential to realistic predictions for the two-phase flows under consideration [7, 8, 18, 19].

2.4.1. *Equation of state.* The Nobel-Abel dense-gas law, also called the Clausius equation,

$$p\left(\frac{1}{\rho_1}-b\right)=\bar{R}T_1, \quad (9)$$

is used as the equation of state for the gas phase, where $\bar{R}$ is the specific gas constant (286.69 J kg^{-1} K^{-1}); and b is the co-volume which is a function of gas density. For the reported results, b is taken as constant.

The statement of a constant density for the solid particles serves as the equation of state for the particles.

2.4.2. *The intergranular stress.* The constitutive law used for the intergranular stress calculation is

$$\begin{aligned}&\tau=0 && \text{for } 0\leqslant R_2\leqslant R_{2,\text{crit}},\\ &\tau=K(R_2-R_{2,\text{crit}}) && \text{for } R_{2,\text{crit}}<R_2\end{aligned} \quad (10)$$

where $R_{2,\text{crit}}$ is a 'critical' volumetric fraction, below which there is no direct contact between particles, and K is a constant, representing the rate of change of stresses with respect to R_2, known from the properties and shape of the particles.

2.4.3. *The interphase-friction coefficient.* Prescribed functions for the coefficient in the drag terms of equations (4), (6) and (7) are used. The expression for the interphase friction force for the finite-difference cell used is a linear one,

$$F=f|U_1-U_2| \quad (11)$$

where U refers to any velocity component, and the interphase friction factor, f, is expressed as

$$f=C_{f,ip}R_1R_2V \quad (12)$$

where $C_{f,ip}$ is a constant estimated from the drag coefficient expression for spherical particles [20]. This simple method has been chosen because of lack of empirical correlations for the problems in question, and requires improvement if accurate results are to be obtained.

2.4.4. *The particle burning-rate.* For the burning-rate law, a simple pressure-dependent relation was employed, namely

$$\dot{b}=\varepsilon\left(\frac{p}{p_{\text{atm}}}\right)^n \quad (13)$$

where p_{atm} is the atmospheric pressure and ε and n are constants.

The production rate of gases from solid particles, $\dot{m}_{21}$, is therefore given by

$$\dot{m}_{21} = \dot{b}A_s \tag{14}$$

where A_s is the total surface area of particles in a control cell, calculated from the following expression, for spherical particles

$$A_s = 6R_2V/[D_0(R_2/R_2^*)^{1/3}] \tag{15}$$

where D_0 is the initial diameter of unburnt particles.

2.4.5. *Ignition criterion.* The criterion for particle ignition used in this study assumes ignition to have occurred when the surface temperature of a particle reaches a critical value, e.g.

$$\begin{aligned} \dot{b} &= 0 && \text{for } T_s < T_{ign}, \\ \dot{b} &= \varepsilon\left(\frac{p}{p_{atm}}\right)^n && \text{for } T_s \geqslant T_{ign}. \end{aligned} \tag{16}$$

The surface temperature of the particles is determined as outlined below.

2.4.6. *The interphase-heat-transfer coefficients.* Although the equations solved for the transport of heat between the gas- and particle-phases are those of the phase enthalpies [equations (6) and (7)], it is convenient to think in terms of temperatures T_1 and T_2, by introduction of the specific heats C_1 and C_2. For simplicity, C_1 and C_2 are assumed equal ($=C$).

Central to the following treatment is the concept of an interface between the two phases, with temperature T_s. Then

$$\dot{q}_{1s} = a_1(T_1 - T_s), \tag{17}$$

$$\dot{q}_{s2} = a_2(T_s - T_2), \tag{18}$$

$$\begin{aligned} \dot{m}_{21} &= 0 && \text{for } T_s < T_{ign}, \\ \dot{m}_{21} &= f(p) && \text{for } T_s \geqslant T_{ign} \end{aligned} \tag{19}$$

where a_1 and a_2, are heat-transfer coefficients multiplied by the interface area through which the transfer occurs; and $f(p)$ is the function given by equation (16) above. An energy balance over a control volume enclosing the interface yields:

heat coming into the control volume $= \dot{q}_{1s} + \dot{m}_{21}CT_2$,

heat going out of the control volume $= \dot{q}_{s2} + \dot{m}_{21}CT_s$,

generation $= \dot{m}_{21}h_c$.

Therefore,

$$\dot{q}_{s2} - \dot{q}_{1s} = \dot{m}_{21}[h_c - C(T_s - T_2)]. \tag{20}$$

Combination of equations (17), (18) and (20) yields

$$T_s = [a_2T_2 + a_1T_1 + \dot{m}_{21}(h_c + CT_2)]/\zeta, \tag{21}$$

$$\dot{q}_{1s} = \frac{a_1}{\zeta}[a_2(T_1 - T_2) + \dot{m}_{21}C(T_1 - T_2) - \dot{m}_{21}h_c], \tag{22}$$

$$\dot{q}_{s2} = \frac{a_2}{\zeta}[a_1(T_1 - T_2) + \dot{m}_{21}h_c] \tag{23}$$

where

$$\zeta = a_1 + a_2 + \dot{m}_{21}C. \tag{24}$$

The heat-transfer coefficient per unit area, a_1''', is estimated by assuming Nusselt number $Nu = 2$, in the absence of any concrete experimental evidence. A better assumption might have been the Denton correlation, as used in ref. [18]. Then,

$$a_1 = a_1'''A_s. \tag{25}$$

The heat-transfer coefficient a_2 is computed assuming a cubic temperature distribution within the particle,

$$a_2 = \frac{3\lambda}{\delta} = 3\lambda/\tfrac{5}{4}D\left\{1 - \left[1 - \frac{8}{5}\left(\frac{T_2 - T_\infty}{T_s - T_\infty}\right)\right]^{1/2}\right\} \tag{26}$$

where D is the particle diameter, T_∞ is the initial temperature at its centre, and δ is the thermal wave penetration depth in a spherical particle, calculated at each time step as described in the Appendix.

2.4.7. *The movement of the projectile.* The projectile velocity and acceleration were calculated at every time step from the computed force, F, acting on its base,

$$F = (p_f - p_b)A \tag{27}$$

where p_f, p_b and A are the projectile frictional pressure, the calculated pressure at its base, and its cross-sectional area, respectively.

3. THE FINITE-DOMAIN EQUATIONS AND THE SOLUTION PROCEDURE

3.1. *Finite-domain equations*

A conventional staggered grid is used [13]. The velocities are stored at the centre of the cell faces to which they are normal; all other variables are stored at the centres of the cells themselves.

The velocity locations have their own surrounding cells, which act as control volumes over which the differential momentum equations are integrated, to yield the corresponding finite-domain equations for velocity. Equations for the other dependent variables employ control volumes around the grid points.

The result of the integration is a set of finite-domain equations of the general form

$$\phi_p = \frac{\sum_i a_i\phi_i + b}{\sum_i a_i - c} \tag{28}$$

where ϕ can stand for any dependent variable. The coefficients a_i represent the effects of convection and diffusion, and $(b + c\phi_p)$ represents the integrated source terms for the cell. The use of upwind-differencing in evaluating the convection terms ensures that the a_i coefficients are always positive, for numerical stability. A fully-implicit formulation is used.

3.2. *Solution method*

The finite-domain equations are solved using the SIMPLEST and IPSA algorithms [13, 14, 17]. The integration proceeds along the axis of the gun barrel from the bottom to the top, and is repeated until convergence is achieved. Further details may be found in the above references.

4. COMPARISON WITH OTHER METHODS

The differential equations presented above differ from those of previous authors in several respects. In particular:

(a) The gas pressure-gradient term is included in the solid-phase momentum equation. Hughes [15] has argued that such a term results in the mechanical set being non-hyperbolic. Krier and Kezerle [12] adopted that argument and, in order to obtain solutions to the equations, found it necessary to neglect the above terms. However, the present work proves that stable and meaningful results can be obtained when solving the full equations.

(b) The pressure gradient term is written as the partial gradient of pressure and not as the gradient of a partial pressure.

(c) A solid-phase energy equation is used, symmetric with the gas-phase energy equation, instead of the common approach of solving the unsteady heat conduction equation for the solid particle and monitoring the heat gained from the gas in the form of convective heat transfer [8, 10, 16]. The latter approach was not deemed acceptable for the present work, for reasons discussed in refs. [12, 18].

A fully-implicit finite-difference scheme was employed for the numerical solutions, with none of the limitations on the choice of time-step imposed by the explicit methods used by previous authors [12].

5. COMPUTATIONAL DETAILS

5.1. *The problem considered*

The problem considered for computation is that of predicting the time-dependent, two-phase mixing, heat-transfer and combustion processes occurring in the gun barrel illustrated in Fig. 1, during a short time period, immediately after ignition. Table 2 summarises the input used to carry out the typical results presented below, including initial conditions.

The problem is specified after a time chosen at $t = 0$, at which an ignition stimulus is imposed by the inflow of hot gases through four nozzles of the ignitor, in a cruciform arrangement. This 'ignition' region was taken to be 40% of the total initial domain length. The heat transfer from the hot gases to the particles raises the particle-surface temperature, until the ignition temperature is reached, initiating combustion. Diffusion effects and wall-friction are assumed negligible.

Table 2. Input data used in the numerical computations

Parameter	Value
Physical properties	
Density of gas, ρ_1	0.861 kg m^{-3}
Density of propellant particles, ρ_2	1500 kg m^{-3}
Specific heat ratio of gas γ	1.27
Specific gas constant, R	286.69 J kg^{-1} K^{-1}
Ignition temperature, T_{ign}	400 K
Chemical energy of propellant, h_c	4 MJ kg^{-1}
Specific heat of gas and propellant, C	2000 J kg^{-1} K^{-1}
Thermal conductivity of solid particles, λ	0.2 kg ms^{-3} K^{-1}
Mass inflow rate of gas from ignitor, $\dot{m}_{IN}$ (at 90° intervals)	20 kg s^{-1}
Period of inflow from ignitor, t_{IN}	5 ms
Temperature of gas from ignitor, T_{IN}	2000 K
Constitutive relations	
Co-volume of gas, b	10^{-3} m^3 kg^{-1}
Propellant burning-rate proportionality constant, ε	0.2 kg m^{-2} s^{-1}
Propellant burning rate index, n	0.9
Intergranular stress proportionality constant, K	1.76×10^8 N m^{-2}
Interphase friction parameter, $C_{f,ip}$	10^6
Interphase heat transfer parameter on the gas-side, a_1	50 W K^{-1}
Critical volume fraction, R_{crit}	0.5
Initial conditions	
Pressure, p	1.0135×10^5 N m^{-2}
Bulk temperature of solid particles, T_2	294 K
Temperature at the centre of a particle, T_∞	294 K
Temperature of gas, T_1	294 K
Volume fraction of solid, R_2	0.5
Velocities of gas and particles, u_1, u_2, v_1, v_2, w_1, w_2	0.0 m s^{-1}
Initial hydraulic particle diameter	2×10^{-4} m
Other input	
Projectile frictional pressure	1 MPa
Projectile mass	4 kg

5.2. *Finite-domain grid and time-step used*

All the computations reported below have been carried out with a finite-domain grid having $5 \times 5 \times 20$ control cells in the θ, r and z directions, respectively. The distribution of grid cells, shown in Fig. 2, is uniform in the θ and r directions, and non-uniform in the z direction, more grid cells being concentrated near the base of the projectile. The integration domain covers only one 45° sector of the barrel cross-section, because of symmetry.

The inflow region, which provides the major contribution to the 3-dim. effects, consisted of the first four cells along the axis, and was spread over one cell in both radial and circumferential directions.

Following the projectile movement, the above grid was allowed to expand in the axial direction at every time-step, to follow the increase in domain length. No grid-dependency tests were performed at this stage. Earlier work, for a 1-dim. problem [19], indicates that the above grid may not be adequate for obtaining grid-independent results. It also indicates that the

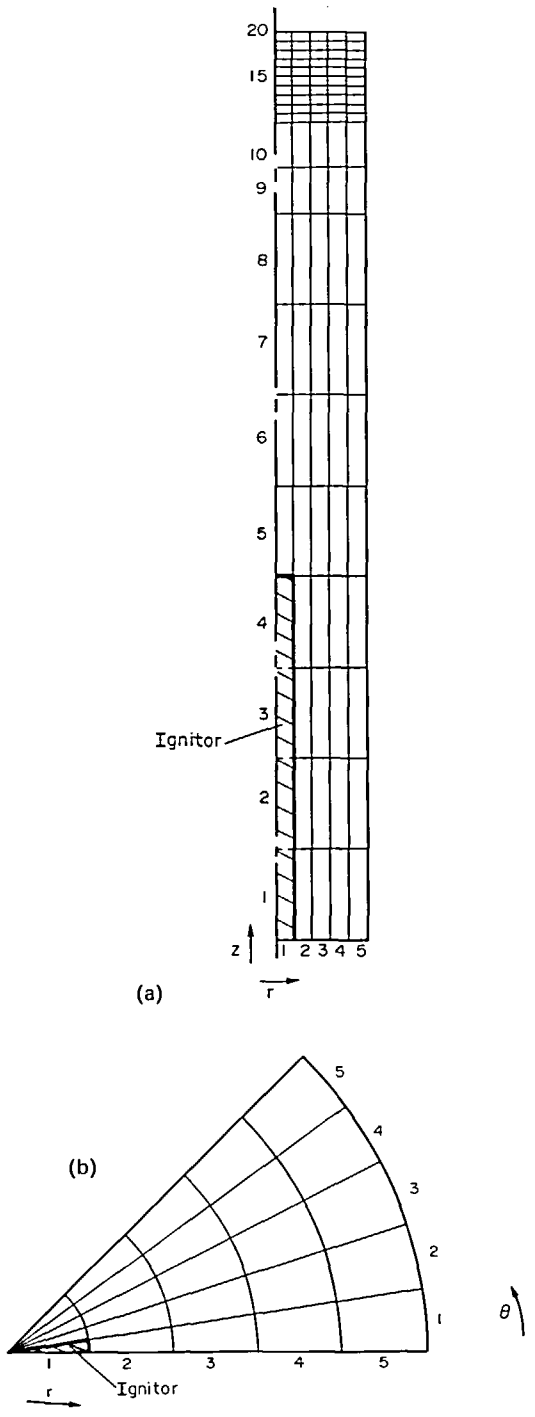

FIG. 2. The solution domain and the finite domain grid used.

dependency of the results on the time-step is much stronger than on the grid; and therefore priority was given to performing a series of time-step dependency computations.

This revealed that, although large time steps can be employed and convergence still obtained, a short time-step of 0.025 ms is required to ensure time-step independency of the results; and this is the time-step used to obtain the presented results.

5.3. *Convergence and computer requirements*

For the results reported, convergence was excellent, with no form of relaxation used. Ten sweeps per time-step were sufficient to ensure good convergence.

In general, the cpu time required per cell, per sweep, per variable, per time-step was 3.0×10^{-3} s on a minicomputer (Perkin-Elmer 3220) which is roughly 16 times slower than an IBM 30/32 machine. A fully-converged run, using the above grid, required $5\frac{1}{2}$ h on the same machine for 100 time steps (roughly 20 min on an IBM 30/32).

6. RESULTS

6.1. *Presentation of the results*

Many results were obtained during the present study but space considerations dictate that only a fraction of these can be presented.

Figures 4–17 present axial, radial and circumferential distribution histories of the fluid-dynamic and heat-transfer variables in the 3-dim. gun barrel of Fig. 1, with an initial solid loading of 50%. Other pertinent input data to the calculations are indicated in Table 2.

Radial distributions are presented at two selected axial sections, namely at axial locations 0.25 L and 0.875 L from the bottom, where L is the length of the barrel.

Circumferential distributions are also presented at the above axial locations, at planes $\theta = 4.5°$ and 40.5° (Fig. 2). The latter were chosen because they present the most significant 3-dim. effects. When no significant variations are observed, a single plot is presented for both θ-planes above.

The figures present the pressure distribution over the barrel as time progresses, the gas and particle velocities, the solid volume fraction, the temperature histories of both phases and the projectile velocity and acceleration histories. Distances on the figures are normalised and the length of the domain as a function of time is given in Fig. 3. Pressure and temperature graphs are presented on logarithmic scale.

6.2. *Discussion of results*

Figure 4 shows the calculated axial pressure distributions at nine different times (i.e. 0.2, 0.4, 0.52, 0.62, 0.72, 1.16, 1.52, 2.02, and 3.02 ms after ignition), at a radial distance of 0.01 m from the axis and at $\theta = 4.5°$.

Beginning with the trace $t = 0.2$ ms, the predictions indicate a rapid build-up of pressure at the lower parts of the barrel, leading to steep pressure gradients. A peak pressure of 2.42×10^9 N m^{-2} is predicted at $t = 1.20$ ms, at a distance of 0.60 m from the bottom of the gun. The pressure level then decreases as the projectile moves forward, and the gas-space increases. Figures 5 and 6 present the calculated radial pressure distributions at six different times (i.e. 0.2, 0.4, 0.52, 1.02, 1.52 and 2.02 ms), at two circumferential locations

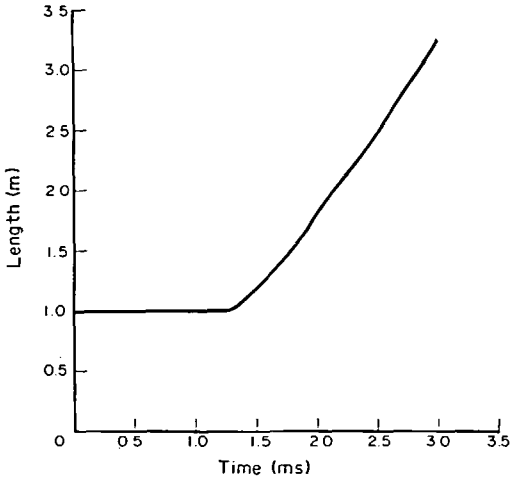

FIG. 3. Length of solution domain vs time.

($\theta = 4.5°$ and 40.5°), and at two axial locations, i.e. near the bottom and near the top of the barrel. Significant radial effects are observed only near the bottom of the barrel (Fig. 5), where the predictions indicate a build-up of pressure over the radial extent of the ignition zone, shortly after ignition, as expected. For times later than 0.55 ms after ignition the pressure becomes more or less uniform in the radial direction. Circumferential effects are observed only near the bottom of the gun barrel and only for a very short period after ignition. These effects are however much less significant than the radial ones, even near the bottom of the barrel.

At the higher axial location (Fig. 6) the predictions indicate a build-up of pressure as time increases, which is more or less uniform in both the radial and circumferential direction.

Figure 7 presents the particle-volume-fraction axial distribution history, at a radial distance of 0.01 m from the axis and at $\theta = 4.5°$. These distributions are given at the same nine different times after ignition, as for the pressure distributions. The particle-volume-fraction profiles show that near the lower end of the barrel the porosity increases fairly rapidly. This is due to both a reduction in volume of the particles due to burning and the forward motion of these particles being carried along by the gas, and to the injection of gas by the ignitor during the first 5 ms. It is this injection of hot gas which ignites and displaces the powder, as can be seen from the considerable positive particle velocities after 1 ms from ignition (Fig. 14). The forward drag on the particles, however, is not sufficient to result in their compaction further downstream, to loadings signifi-

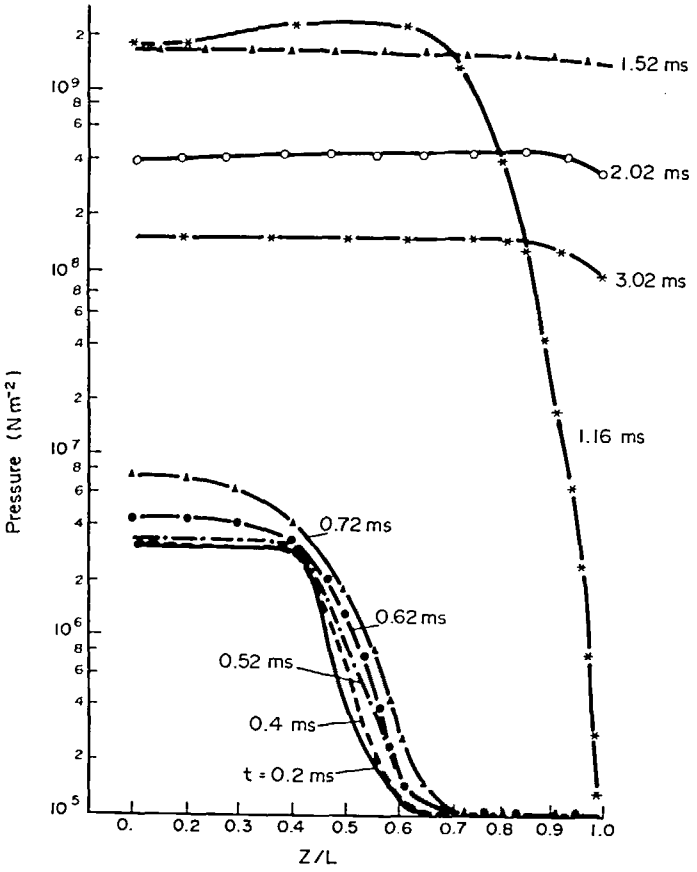

FIG. 4. Pressure axial distribution history, at $r = 0.01$ m and $\theta = 4.5°$ (logarithmic scale).

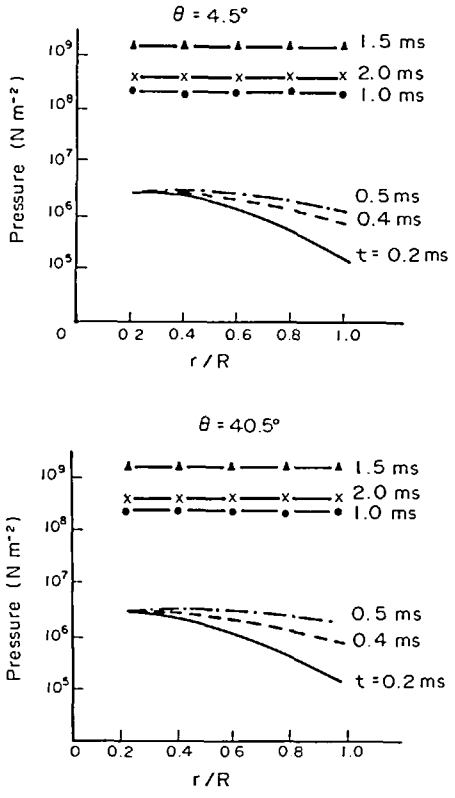

FIG. 5. Pressure radial and circumferential distribution histories at $z = 0.25L$ (logarithmic scale).

cantly greater than the original 50%. (A maximum of about 50.1% is observed.) The rapid decrease in particle volume fraction near the top of the barrel at times greater than $t = 1.20$ ms is caused by the movement of the projectile, which drags the gas with it, displacing the powder (Figs. 13 and 14), and the penetration of the flame front at the higher elevations of the barrel, causing combustion.

Strong 3-dim. effects can be seen in the particle-volume-fraction radial and circumferential histories, at the axial location near to the bottom of the barrel (Fig. 8). Thus, near the symmetry axis, where injection occurs, the particle-volume-fraction attains very low values, which increase as we move towards the outer barrel wall. This is caused by the inflow of the hot gas from the ignitor, displacing and burning the particles. Nearly all particles have burnt within 1.5 ms from ignition, at this axial station.

The particles are actually compacted uniformly at the higher values of radius to loadings of 52%, at $\theta = 4.5°$. The significant circumferential effects may be seen by comparing the two plots of Fig. 8 ($\theta = 4.5°$ and $\theta = 40.5°$). At $\theta = 40.5°$, the particles are compacted to loadings of up to 59% all over the radial extent of the barrel, for times up to about $t = 0.5$ ms, when they also start burning. There is a delay in burning at the above two circumferential locations of about 0.9 ms.

Such 3-dim. effects are not observed further downstream of the ignition stimulus, and at an axial

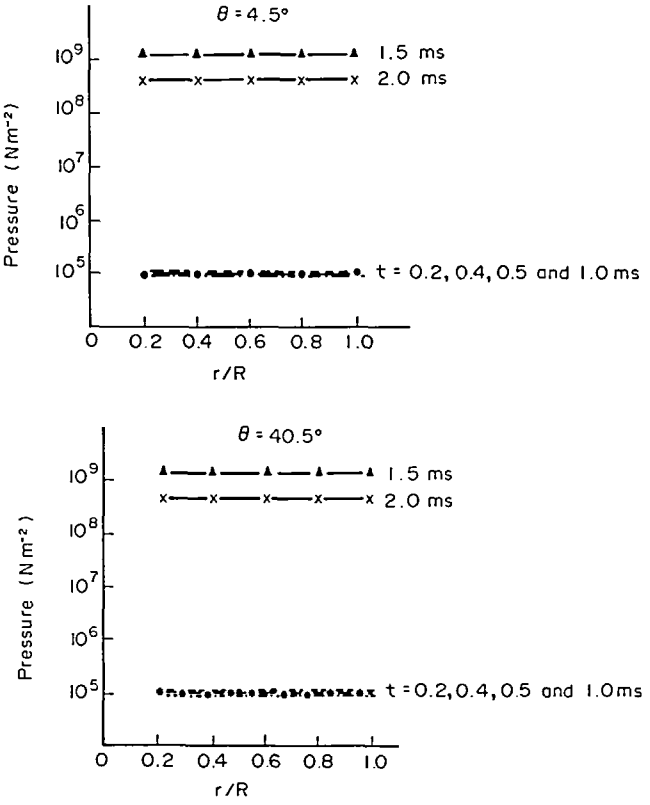

FIG. 6. Pressure radial and circumferential distribution history at $z = 0.875L$ (logarithmic scale).

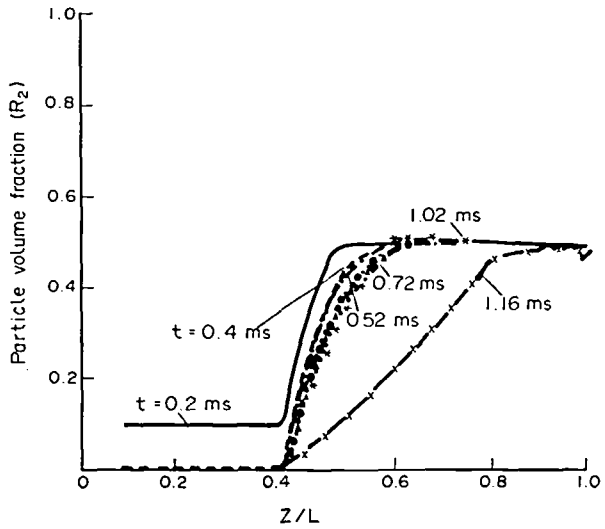

FIG. 7. Particle volume-fraction axial distribution history at $r = 0.01$ m and $\theta = 4.5°$ (for $t > 1.52$ ms nearly all particles have been burnt).

location of $0.875\,L$ from the bottom (Fig. 9) the particle-volume-fraction distributions are independent of radius and angle. The particles retain their initial loading of 50% up to about $t = 1.00$ ms, when they start burning, more or less uniformly.

Figures 10 and 11 present gas-temperature and particle-temperature axial distribution histories at eight selected times after ignition (0.2, 0.4, 0.52, 0.62, 0.72, 1.52, 2.02, and 3.02 ms). Due to combustion, the gas temperatures are generated at very high values, around 2500 K, and as the pressure increases, the gas is compressed to even higher values (3400 K). These temperatures decay rapidly further downstream, up to times of 1 ms after ignition, as the gas loses heat to the

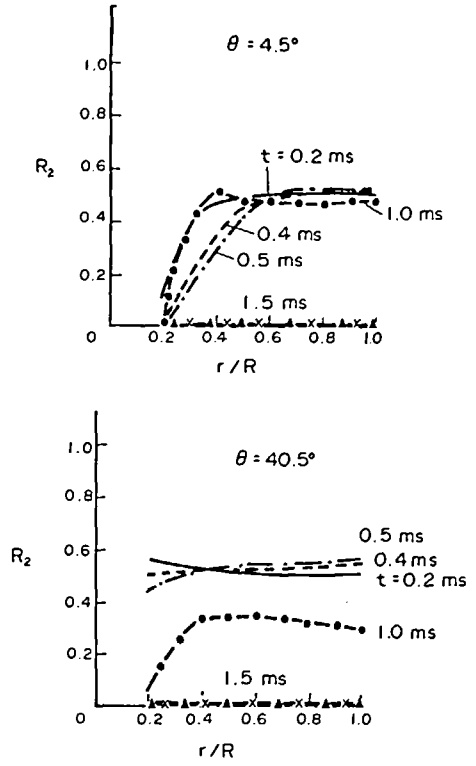

FIG. 8. Particle volume-fraction radial and circumferential distribution histories at $z = 0.25L$.

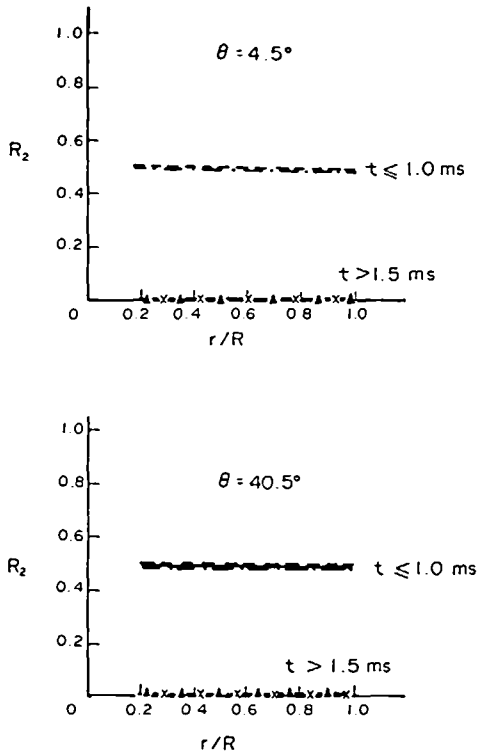

FIG. 9. Particle volume-fraction radial and circumferential distribution histories at $z = 0.875L$.

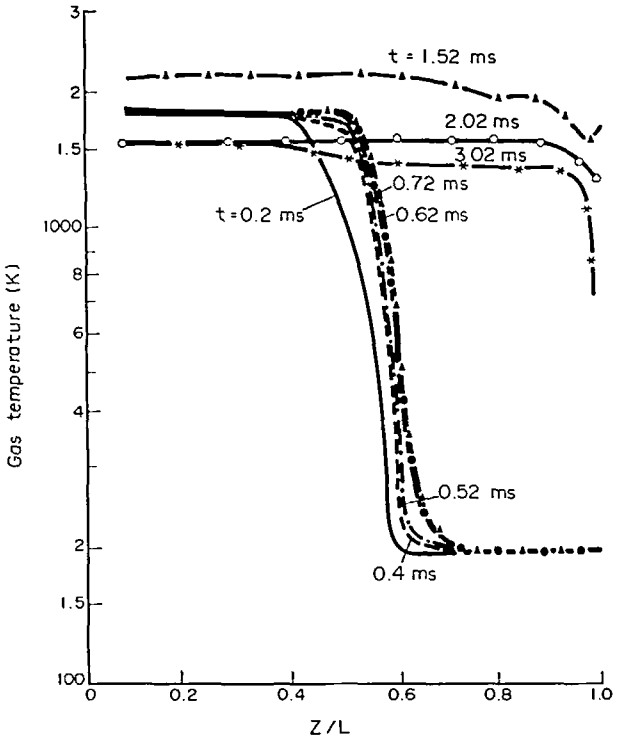

FIG. 10. Gas-temperature axial distribution history at $r = 0.01$ m and $\theta = 4.5°$ (logarithmic scale).

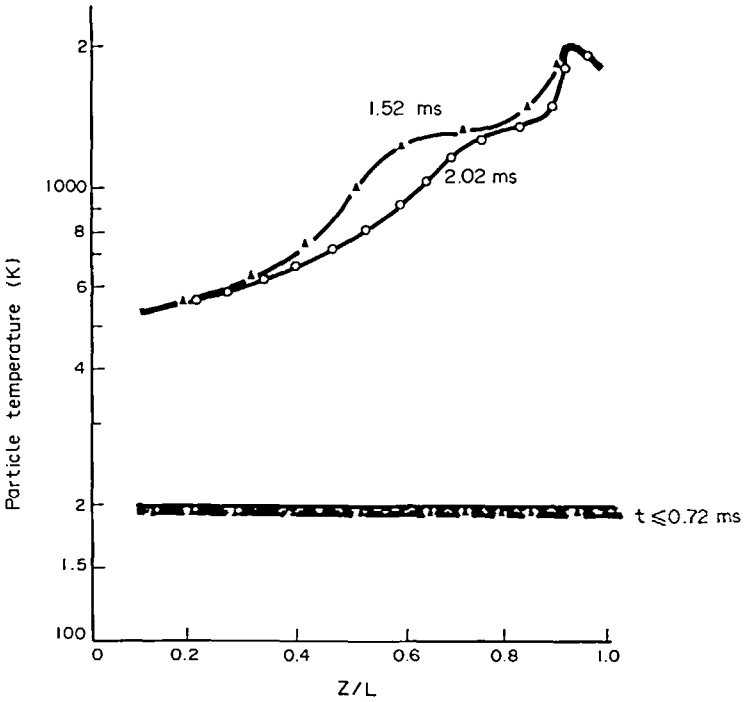

FIG. 11. Particle-temperature axial distribution history at $r = 0.01$ m and $\theta = 4.5°$ (1. logarithmic scale, 2. at $t = 2.02$ ms very few particles remain).

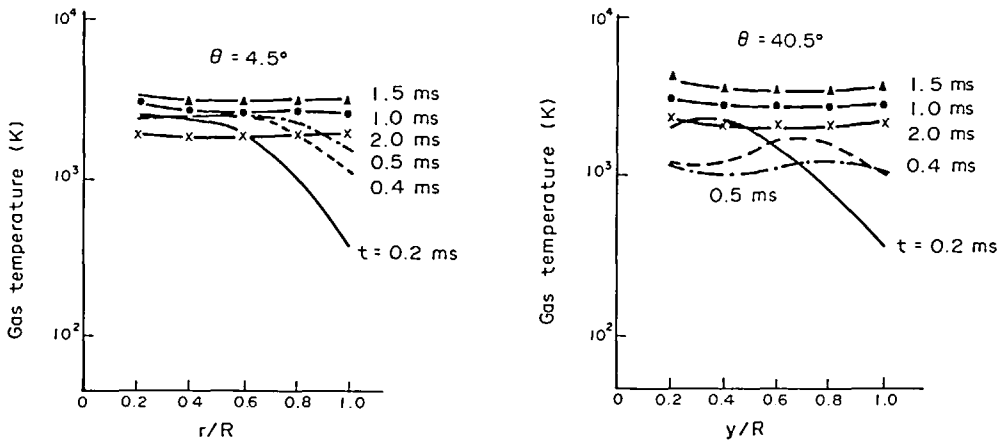

FIG. 12. Gas-temperature radial and circumferential distribution histories at $z = 0.25L$ (logarithmic scale).

solid by convection into the bed interior. The high gas-temperature front starts travelling rapidly up the barrel, igniting the powder after about 1 ms. The flame front reaches the far downstream region of the barrel at about 1.3 ms.

The temperature level drops after the projectile starts moving, thus causing a decrease in pressure. This drop is much more pronounced just behind the accelerating projectile, at $t = 3$ ms.

The particle temperatures (Fig. 11), remain more or less uniform, at around 300 K, up to $t = 0.72$ ms and then rise steeply to a maximum of around 3100 K just behind the projectile at $t = 1.5$ ms, as burning spreads downstream. Subsequently, the temperatures of the few remaining particles decrease as the projectile starts accelerating, thus causing a decrease in pressure and temperature. Strong 3-dim. in the gas-temperature distributions is indicated in Fig. 12, which presents the radial and circumferential temperature history at the lower part of the barrel. Such three-dimensionality is not evident at the upper elevations of the barrel. On the contrary, the particle temperature distributions are

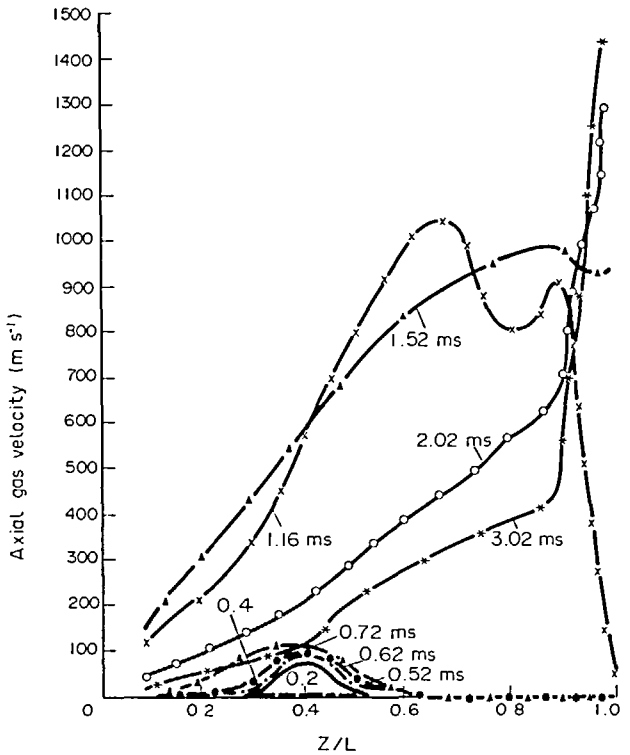

FIG. 13. Axial distribution history of axial gas-velocity at $r = 0.01$ m and $\theta = 4.5°$.

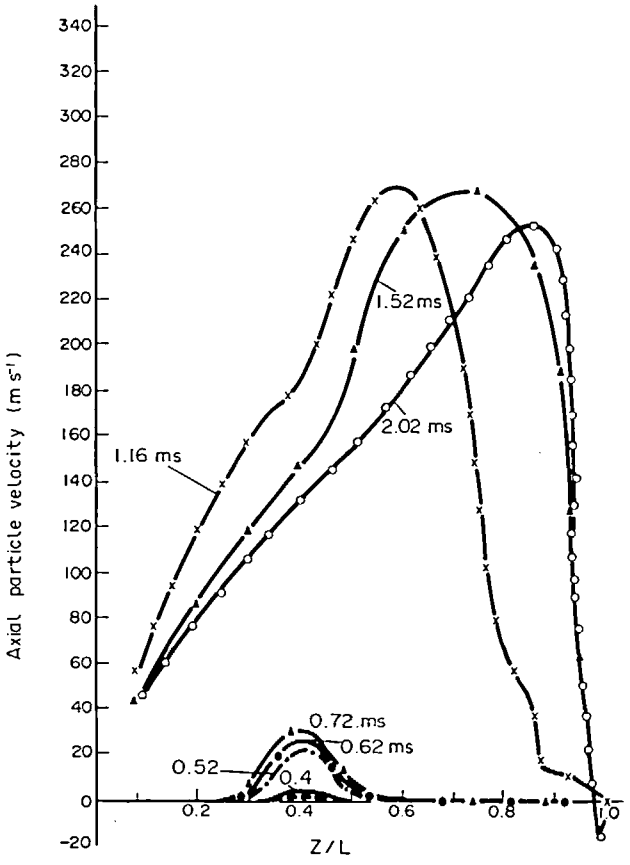

FIG. 14. Axial distribution history of axial particle-velocity at $r = 0.01$ m and $\theta = 4.5°$ (nearly all particles are burnt at $t = 2.02$ ms).

more or less uniform in the radial and circumferential directions at every elevation in the barrel, and for all times studied. The computed high gas temperatures are due to the assumptions of constant specific heat and that all gases obey the Noble–Abel equation of state. These assumptions preclude the flow of energy into dissociation of the gaseous combustion products. The high particle temperatures predicted at later times are a consequence of the surface-to-volume ratio increasing inversely with particle diameter, as the particles burn out. Therefore, the particle temperature means very little as $R_1 \to 1.0$, but then, its value does not influence the convective flame spreading in any significant way.

Figures 13 and 14 present gas- and particle-axial velocity distributions at the chosen times. A peak is observed in both gas and particle profiles up to $t = 0.72$ ms, driven by the pressure gradient. Subsequently, the peak is retained by the particle profiles, but not by the gas velocities which obtain their maximum just behind the projectile, as it drags the gas with it. Worth noting are the extreme gas velocities, sometimes exceeding 1000 m s^{-1}, and the considerable slip between gas and propellant particles. The particle velocities are in general much lower than the gas velocity (max. 270 m s^{-1}), since the inertia of the particles is greater than that of the gas.

Figures 15 and 16 present radial and circumferential distributions of the particle- and gas-axial velocity at the chosen times, at $z = 0.25\ L$.

The effect of inflow of hot gas from the ignitor is seen in Fig. 15 which presents the radial distribution of the particles axial velocity. The hot gas inflow at $\theta = 4.5°$ causes particles to accelerate axially, particularly near the axis.

The strong three-dimensionality in the particles axial velocity diminishes further downstream. Figure 16 presents the corresponding axial velocity profiles of the gas phase. Strong slip between the phases is observed, and the three-dimensionality, evident in the gas profiles at the lower elevation, persists further downstream, although significantly diminished.

Projectile acceleration and velocity histories are presented in Fig. 17. It is seen that the projectile starts moving at around $t = 1.2$ ms and accelerates rapidly to a peak value of 6.6×10^5 m s^{-2} at $t = 1.32$ ms, when it attains a velocity of 680 m s^{-1}. Subsequently, the projectile acceleration diminishes, as the domain expands and the driving force at its base decreases, whilst the velocity continues to increase to values of 1500 m s^{-1} at $t = 3$ ms. The acceleration of the projectile produces a 10% length expansion in 1.40 ms, and a 100% length expansion in 2.20 ms.

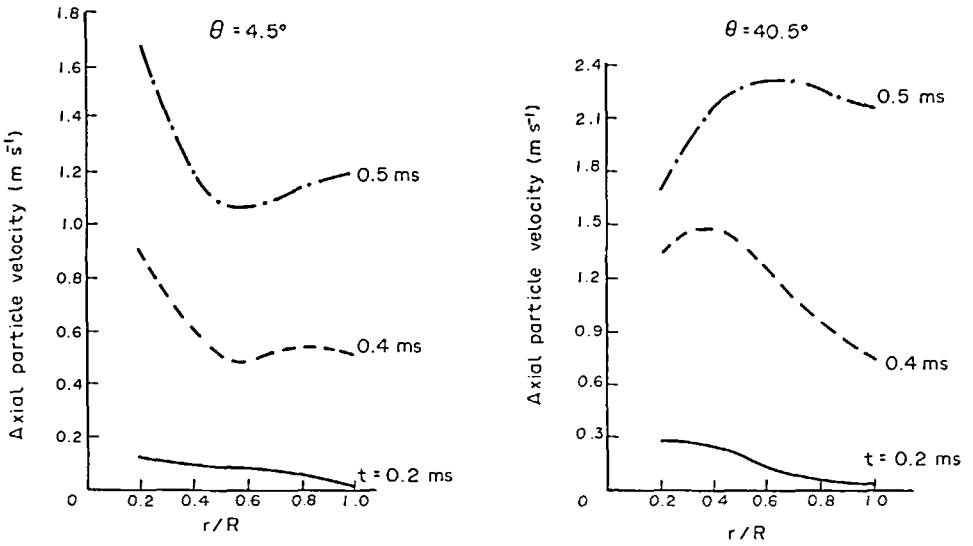

FIG. 15. Radial and circumferential distribution histories of axial particle velocity at $z = 0.25L$.

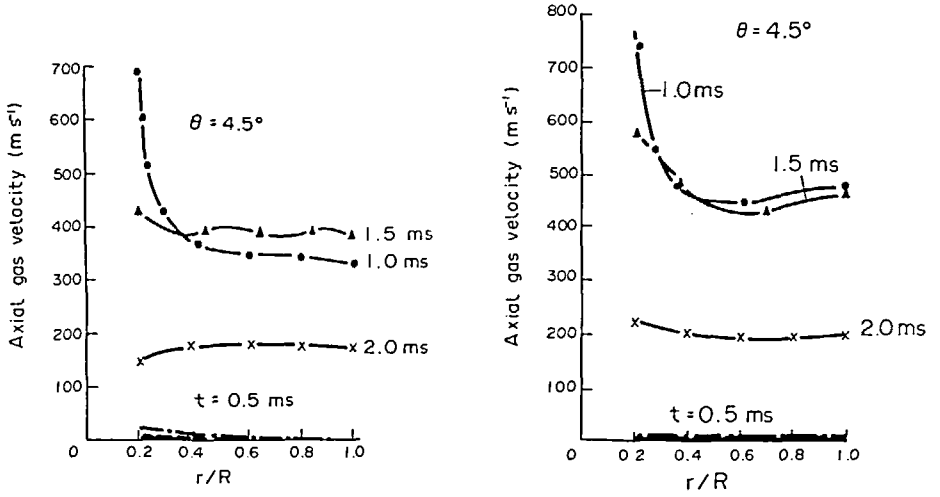

FIG. 16. Radial and circumferential distribution histories of axial gas velocity at $z = 0.25L$.

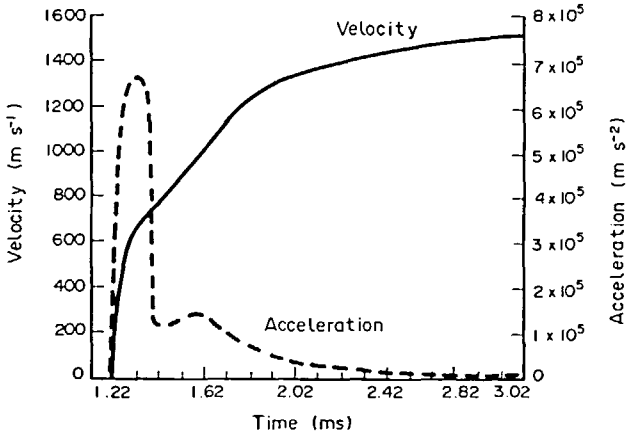

FIG. 17. Projectile acceleration and velocity histories.

7. CONCLUSIONS

A theoretical model has been developed, and used to predict the combustion of mobile granular propellants in gun barrels. A stable, fast-converging numerical scheme was used for solving the complete system of equations. The procedure is general, and allows two-phase, 3-dim. transient computations to be performed on minicomputers.

Results have been presented and their nature appears realistic. At present these results cannot be quantified in detail because of the unsatisfactory empirical input, particularly for the interphase friction coefficient. The transient wave phenomena and flame spreading are predicted by the present model, which indicates that the rate of pressurisation increases in the downstream direction and the pressure peak developed in the gun barrel travels downstream. These findings are consistent with expectations and the existing, very limited, experimental evidence.

The reported work confirms the argument that the mathematical formulation of two-phase gun barrel phenomena is satisfactory, and that the solution procedure is both reliable and practicable. There are no known problems associated with the mathematical model. The remaining problems are associated with the physical processes of the two-phase flows, namely the heat-, mass-, and momentum-transfer between the phases.

The choice of relevant interphase parameters has a profound effect on the results, as was proved by an extensive study on varying the parameters given in Section 2 above, in the context of other unpublished work. This is also the conclusion given in ref. [18]. Much more work is therefore required to obtain reliable experimental correlations on the above processes, which can then be used to improve the input of the present model.

REFERENCES

1. D. B. Spalding, The calculation of free-convective phenomena in gas–liquid mixtures, in *Proc. ICHMT Seminar*, Dubrovnik, Yugoslavia, p. 569. Hemisphere, Washington (1976).
2. N. C. Markatos, A. Moult, P. J. Phelps and D. B. Spalding, The calculation of steady, three-dimensional, two-phase flow and heat transfer in steam generators, in *Proc. ICHMT Seminar*, Dubrovnik, Yugoslavia, pp. 485–502. Hemisphere, Washington (1978).
3. Yu. A. Buyevich, Statistical hydromechanics of disperse systems—1: Physical background and general equations, *J. Fluid Mech.* **49**, 498–507 (1971).
4. Yu. A. Buyevich, Statistical hydromechanics of disperse systems—2: Solution of the kinetic equation for suspended particles, *J. Fluid Mech.* **52**, 345–355 (1972).
5. Yu. A. Buyevich, Statistical hydromechanics of disperse systems—3: Pseudo-turbulent structure of homogeneous suspensions, *J. Fluid Mech.* **56**, 313–336 (1972).
6. H. Krier, W. Van Tassel, S. Rajan and J. T. Vershaw, Model of gun propellant flame spreading and combustion, BRL CR 147, Ballistic Research Laboratories, Aberdeen Proving Ground, Maryland; *Int. J. Heat Mass Transfer* **18**, 1377–1386 (1975).
7. H. Krier and S. Rajan, Flame spreading and combustion in packed beds of propellant grains, AIAA 13th Aerospace Sciences Meeting, Pasadena, California, Paper No. 75-240.
8. P. S. Gough, Fundamental investigation of the interior ballistics of guns, Final Report IHCR 74-1, Naval Ordnance Station, Indian Head, Maryland (1974).
9. K. K. Kuo, R. Vichnevetsky and M. Summerfield, Theory of flame front propagation in porous propellant charges under confinement, *AIAA Jl* **11**, 444–451 (1973).
10. K. K. Kuo, J. H. Koo, T. R. David and G. R. Coates, Transient combustion of mobile gas-permeable propellants, *Acta Astronautica* **3**, 573–591 (1976).
11. J. H. Koo and K. K. Kuo, Transient combustion in granular propellant beds, BRL CR 346, The Pennsylvania State University, Dept. of Mech. Engineering (1977).
12. H. Krier and J. A. Kezerle, Modelling of convective mode combustion through granulated propellant to predict transition to detonation, Technical Report AAE77-17 (UILU-Eng 77 0517), University of Illinois, Urbana, Aeronautical and Astronautical Engineering Dept.; also presented at the 17th Symposium (International) on Combustion. The Combustion Inst., Pittsburgh (1979).
13. D. B. Spalding, Numerical computation of multi-phase fluid flow and heat transfer, in *Recent Advances in Numerical Methods in Fluids* (edited by C. Taylor) Vol. 1, pp. 139–167. Pineridge Press, Swansea (1979).
14. Y. Kurosaki and D. B. Spalding, One-dimensional unsteady two-phase flows with interphase slip: A numerical study, Presented at 2nd Multiphase Flow and Heat Transfer Symposium Workshop, Miami Beach, April (1979).
15. E. D. Hughes, Field balance equations for two-phase flows in porous media, in *Proc. Two-Phase Flow and Heat Transfer Symposium*—1976 (edited by T. N. Veziroglu) University of Miami, October (1976).
16. K. K. Kuo and M. Summerfield, High speed combustion of mobile granular solid propellants, in *Fifteenth Symposium on Combustion*, pp. 515–525. The Combustion Inst., Pittsburgh (1974).
17. D. B. Spalding, Mathematical methods in nuclear-reactor thermal hydraulics, paper presented at the American Nuclear Society Meeting on Nuclear-Reactor Thermal Hydraulics, Saratoga, NY, 6 October (1980).
18. S. S. Gokhale and H. Krier, Modelling of unsteady two-phase reactive flow in porous beds of propellant, *Prog. Energy Combust. Sci.* **8**, 1–39 (1982).
19. N. C. Markatos, Modelling of two-phase, transient flow and combustion of granular propellants, *Int. J. Multiphase Flow* (1983) (in press).
20. C. E. Lapple, Dust and mist collection, in *Chemical Engineering Handbook* (edited by J. H. Perry) (3rd edn.) p. 1018. McGraw-Hill, New York (1950).

APPENDIX

THE COMPUTATION OF PARTICLE SURFACE TEMPERATURE

The following figure presents a solid particle of radius R at a bulk temperature $\bar{T}_2$, surrounded by gas at temperature T_1. Let T_∞ be the initial temperature at its centre, assumed constant, and T_s the surface temperature.

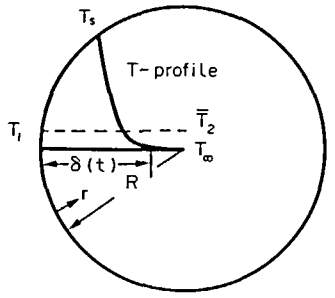

FIG. 18. Definition of various temperatures associated with a solid particle.

The temperature profile within the particle is assumed to be the following cubic function:

$$\frac{T-T_\infty}{T_s-T_\infty}=\left[1-\frac{r}{\delta(t)}\right]^3 \quad \text{for } r \leqslant \delta(t) \tag{A1}$$

where r is measured from the particle surface inwards.

The definition of $\bar{T}_2$ as the bulk particle temperature leads to

$$\bar{T}_2\pi R^2 = 2\pi\int_0^R T(R-r)\,dr, \tag{A2}$$

and after some calculations we finish up with

$$\delta^2-5R\delta+10\left(\frac{\bar{T}_2-T_\infty}{T_s-T_\infty}\right)R^2=0, \tag{A3}$$

which has only one acceptable root,

$$\delta=\frac{5}{2}R\left\{1-\left[1-\frac{8}{5}\left(\frac{\bar{T}_2-T_\infty}{T_s-T_\infty}\right)\right]^{1/2}\right\}. \tag{A4}$$

The satisfaction of the condition $\delta \leqslant R$, requires

$$T_s-T_\infty \geqslant \frac{5}{2}(\bar{T}_2-T_\infty), \tag{A5}$$

which is also a sufficient condition for a real root of equation (A3).

Furthermore,

$$\left(\frac{\partial T}{\partial r}\right)_s=-\frac{3}{\delta}(T_s-T_\infty), \tag{A6}$$

therefore,

$$a_2=\frac{3\lambda}{\delta}\frac{(T_s-T_\infty)}{T_s-\bar{T}_2}\simeq\frac{3\lambda}{\delta}. \tag{A7}$$

$\delta(t)$ is calculated at every time-step by equation (A4) and then a_2 is found from equation (A7), and is used to calculate T_s from equation (21).

ANALYSE ET CALCUL DE L'ECOULEMENT TRIDIMENSIONNEL VARIABLE ET DE LA COMBUSTION A TRAVERS DES PROPERGOLS GRANULAIRES

Résumé—Les propergols solides et perméables aux gaz présentent un grand potentiel de production de poussée élevée pendant un intervalle de temps court.

On présente la formulation théorique et l'application d'un modèle qui décrit le phénomène physique important s'instaurant à la fois dans les phases gazeuse et solide pour constituer les systèmes tridimensionnels, diphasiques, variables et réactifs typiques de la ballistique interne.

Une méthode numérique stable, rapidement convergente et complètement implicite est utilisée pour résoudre les équations aux dérivées partielles non-linéaires couplées de modèle, de façon à permettre au concepteur l'évaluation des effets importants.

Des solutions sont présentées qui évaluent l'onde de pression et le front de flamme en accélération pour un propergol solide granulaire dans l'âme d'un-canon avec un projectile en accélération. Les résultats montrent que le front de flamme s'accélère et que la vitesse de pressurisation augmente substantiellement dans la direction en aval, comme souhaité, et ils sont physiquement raisonnables sous tous les aspects.

UNTERSUCHUNG UND BERECHNUNG DER DREIDIMENSIONALEN INSTATIONÄREN STRÖMUNG UND DES VERBRENNUNGSVORGANGS IN KÖRNIGEN TREIBMITTELN

Zusammenfassung—Gasdurchlässige, feste Treibmittel sind in der Lage, hohen Schub während extrem kurzer Zeitintervalle zu erzeugen. Der Bericht enthält die theoretische Formulierung und die Anwendung eines Modells, welches die wichtigsten physikalischen Phänomene beschreibt, welche in der gasförmigen und festen Phase bei derartigen dreidimensionalen, zweiphasigen, instationären, reagierenden Strömungen auftreten, wie sie in der inneren Ballistik vorkommen. Zur Lösung der gekoppelten, nicht-linearen Gleichungen des Modells wurde eine stabile, schnell konvergierende, voll implizite, numerische Methode angewandt, so daß Einflüsse, die dem mit Problemen der inneren Ballistik befaßten Konstrukteur wichtig erscheinen, untersucht werden können. Die Lösungen beschreiben die Ausbildung der Stoßwelle und die beschleunigte Flammenfront für Festbetten aus körnigen Treibmitteln in Gewehrläufen mit einem beschleunigten Projektil. Die Ergebnisse zeigen, daß die Geschwindigkeit der Flammenfront und die Druckerhöhung in Strömungsrichtung, wie erwartet, erheblich zunimmt. Die Ergebnisse sind in jeder Hinsicht physikalisch sinnvoll.

АНАЛИЗ И РАСЧЕТ ТРЕХМЕРНОГО, НЕУСТАНОВИВШЕГОСЯ ТЕЧЕНИЯ И ГОРЕНИЯ В ОБЪЕМЕ ГРАНУЛИРОВАННОГО ТВЕРДОГО РАКЕТНОГО ТОПЛИВА

Аннотация—Газопроницаемое твердое ракетное топливо может создавать большую реактивную движущую силу за исключительно короткие промежутки времени. Дана теоретическая формулировка и показано использование модели, учитывающей важные физические явления, происходящие в газовой и твердой фазах в таких трехмерных двухфазных нестационарных реагирующих проточных системах, характерных для задач внутренней баллистики. Связанные нелинейные дифференциальные уравнения решаются с помощью устойчивого, быстро сходящегося, полностью неявного численного метода, что позволяет учитывать практически важные эффекты. Полученные решения позволяют рассчитать формирование волны давления и ускоренное движение фронта пламени в слоях гранулированных твердых топлив при движении снаряда в стволе орудия. Как показывают результаты расчетов, распространение фронта пламени значительно ускоряется, а давление существенно возрастает в направлении течения, что является физически правдоподобным.